The past and future of global river ice

https://doi.org/10.1038/s41586-019-1848-1

Received: 31 December 2018

Accepted: 16 October 2019

Published online: 1 January 2020

Xiao Yang[1]*, Tamlin M. Pavelsky[1] & George H. Allen[2]

More than one-third of Earth's landmass is drained by rivers that seasonally freeze over. Ice transforms the hydrologic[1,2], ecologic[3,4], climatic[5] and socio-economic[6–8] functions of river corridors. Although river ice extent has been shown to be declining in many regions of the world[1], the seasonality, historical change and predicted future changes in river ice extent and duration have not yet been quantified globally. Previous studies of river ice, which suggested that declines in extent and duration could be attributed to warming temperatures[9,10], were based on data from sparse locations. Furthermore, existing projections of future ice extent are based solely on the location of the 0-°C isotherm[11]. Here, using satellite observations, we show that the global extent of river ice is declining, and we project a mean decrease in seasonal ice duration of 6.10 ± 0.08 days per 1-°C increase in global mean surface air temperature. We tracked the extent of river ice using over 400,000 clear-sky Landsat images spanning 1984–2018 and observed a mean decline of 2.5 percentage points globally in the past three decades. To project future changes in river ice extent, we developed an observationally calibrated and validated model, based on temperature and season, which reduced the mean bias by 87 per cent compared with the 0-degree-Celsius isotherm approach. We applied this model to future climate projections for 2080–2100: compared with 2009–2029, the average river ice duration declines by 16.7 days under Representative Concentration Pathway (RCP) 8.5, whereas under RCP 4.5 it declines on average by 7.3 days. Our results show that, globally, river ice is measurably declining and will continue to decline linearly with projected increases in surface air temperature towards the end of this century.

River ice, which is widespread at middle to high latitudes and elevations[12,13], regulates many aspects of river functions. For example, river ice contributes to the seasonal ice road network, which serves remote Arctic communities[14]. During the spring melt, ice-jam floods cost about US$300 million in 2017 in North America alone[7]. Although disruptive to humans, ice-jam flooding has an ecologically beneficial role, distributing fresh water, sediments and nutrients to riparian ecosystems[4]. River ice is also thought to regulate greenhouse gas emissions from rivers to the atmosphere by seasonally blocking an estimated 87,000 km^2 of stream surface[5].

Despite the wide-ranging importance of river ice, knowledge of its global extent and change is extremely limited. Three studies have investigated historical river ice extent in the Northern Hemisphere: the first[15] estimated changes in river ice phenology from 1979 to 2009 with a physically based model; the second[12] estimated that 56% of rivers were affected by ice cover, using the 0-°C surface air temperature (SAT) isotherm as a proxy for river ice; and the third study[10] found consistent trends of later surface water freeze-up (5.7 days later per 100 years) and earlier break-up (6.3 days earlier per 100 years) based on long-term records of ice occurrence from 5 rivers and 21 lakes. Various rates of changes have been observed from local to regional records[1,9,16,17], but extrapolating these observations globally is challenging because of poor spatial coverage and, more importantly, the spatially heterogeneous nature of ice dynamics revealed by evaluations of ice break-up dates along river profiles[18,19]. Moreover, trends from in situ observations are inconsistent owing to differences in the definitions of phenological dates, changes in instrumentation and the selection of study sites and analysis periods[9]. Of the few studies that have predicted future changes in river ice extent, most have been based on simple ice–SAT relationships derived from in situ records and conducted at regional scales[11,20]. To accurately project future changes in river ice extent at the global scale, a robust and comprehensive understanding of the relationship between climate and ice extent is required[21].

In this study, we present a global, multitemporal river ice extent dataset, based on 407,880 satellite images from 34 years of observations from the Landsat 5–8 missions (1984–2018). Analysis reveals patterns of change in global river ice cover and enables the development and validation of a simple, yet highly predictive, empirical model of river ice extent. Applying the model to future climate projections, we forecast end-of-century changes in the global extent and seasonal duration of river ice cover.

To construct a global multitemporal river ice extent dataset, we first identified 7.5 million river centreline locations observable by Landsat with a width ≥90 m and a water occurrence ≥90% (refs. [22,23]), largely corresponding to rivers with stream order ≥3 (ref. [24]). To calculate river ice extent, we then extracted snow/ice conditions from the quality band of Landsat images on the Google Earth Engine[25] platform. Snow/ice in the quality band was classified by the US Geological Survey using the Fmask

[1]Department of Geological Sciences, University of North Carolina at Chapel Hill, Chapel Hill, NC, USA. [2]Department of Geography, Texas A&M University, College Station, TX, USA.
*e-mail: yangxiao@live.unc.edu

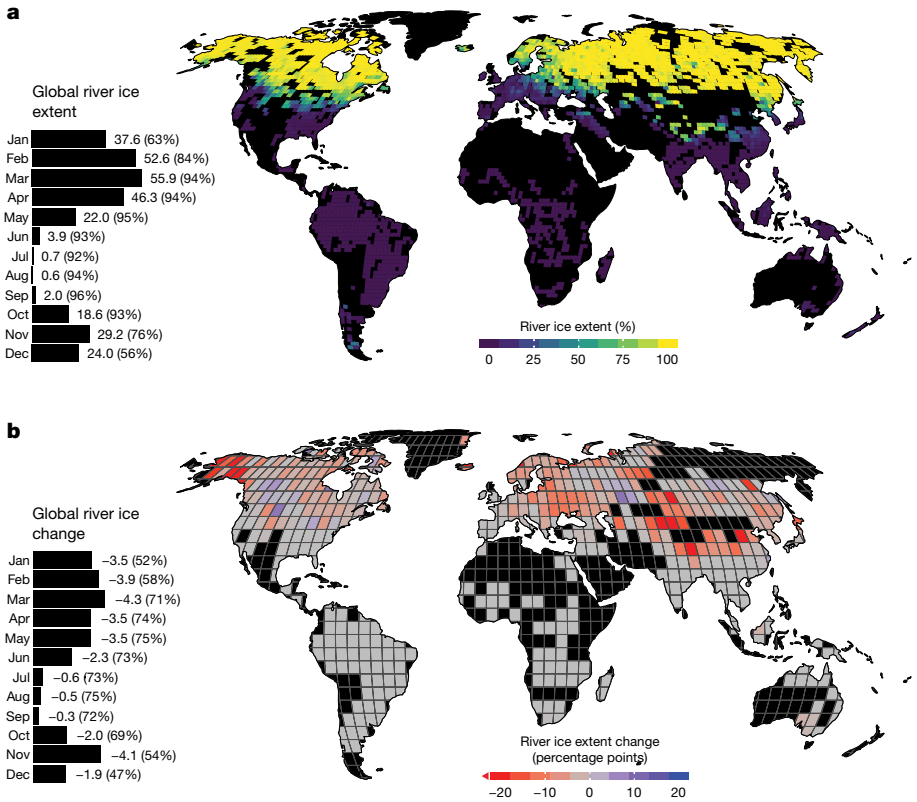

Fig. 1 | Extent of river ice from 1984 to 2018. a, Map of mean river ice extent (in terms of ice-covered length percentage) for the winter season—boreal winter (December, January and February) for the Northern Hemisphere and austral winter (June, July and August) for the Southern Hemisphere. The bar plot shows the monthly percentage of ice-covered rivers globally. The percentage of studied rivers observed successfully by Landsat is shown in parentheses. **b**, Map of changing river ice conditions between 1984–1994 and 2008–2018. Changes were calculated at a 5° × 5° tile scale instead of at the Landsat tile scale used in **a** to increase data availability. The bar plot shows the monthly river ice change with the percentage of studied rivers successfully observed by Landsat in parentheses. In both maps, the black area denotes either insufficient data or a lack of Landsat-observable rivers.

algorithm[26], which labels each pixel as clear, water, cloud, cloud shadow or snow/ice. To reduce the volume of data, we aggregated pixel-level snow/ice conditions into the percentage of total river length covered by ice, or river ice extent, for each Landsat image. To our knowledge, the result constitutes the first global multitemporal quantification of river ice extent.

The main source of uncertainty in the river ice extent dataset comes from the classification error of snow/ice in Fmask. Although the spectral method for classifying snow/ice was adapted from other optical sensors that have been validated[27], the snow/ice classification in Fmask has not previously been systematically evaluated for Landsat images. By comparing Fmask-derived river ice extent to in situ river ice records in Alaska (from the US National Weather Service) and Canada (from the Water Survey of Canada), we estimated the overall accuracy of the Fmask-derived river ice extent to be 0.94 ($P \leq 0.001$; see details in Methods).

Using the global river ice extent dataset, we calculated large-scale river ice coverage and estimated its recent changes. Globally, we esti-mated a maximum ice extent of 56% for the 94% of rivers that were successfully observed in March (Fig. 1a). The distribution of river ice was strongly asymmetric between hemispheres. In the Northern Hemi-sphere, where other studies have estimated the maximum extent of river ice, we found that 66% of the observed river length in March was ice-covered, about 18% higher than previous estimates[12] (note that 4% of the targeted rivers were not successfully observed in March owing to insufficient data). In the Southern Hemisphere, river ice was detected only in New Zealand, the southern tip of the Andes in South America and the southernmost part of Australia. River ice was found at the lowest latitudes in continental regions with high topographies, such as the Rocky Mountains in North America and the Tibetan Plateau in Asia. Conversely, less ice was detected over relatively high latitudes in Western Europe and the Pacific Northwest of the United States, probably because of the influence of nearby ice-free oceans.

Comparing observed river ice cover between 2008–2018 and 1984–1994, we detected a monthly global decline ranging from 0.3 to 4.3 percentage points (Fig. 1b; note that the percentage point change and the percentage change are different—that is, moving from 10% to 7.5% would be a 2.5 percentage point change, but a 25% change). The magnitude of decline was lower during July–September, when river ice is least prevalent. The majority of the changes in the northern mid- to high latitudes are towards less river ice cover, with the greatest declines around the Tibetan Plateau, eastern Europe and Alaska. The monthly river ice change was calculated wherever data were available for both decades (see Extended Data Figs. 1, 2), accounting for 47–75% of the global rivers successfully observed by Landsat, depending on the month.

The observed decline in river ice is likely to continue with predicted global warming. By matching the river ice extent dataset with a 30-day prior mean SAT from the ERA5 climate reanalysis dataset[28], we demonstrate that river ice extent can be accurately represented, based on temperature and season, by a logistic regression model (Fig. 2a; root-mean-square error, RMSE: 13.8 percentage points; mean bias (MBS), 0.6 percentage points). Within the critical temperature range (−10 °C to 10 °C) for ice–water transition, our model reduced the RMSE by 30% and MBS by 87% compared with the 0-°C-isotherm model (Fig. 2b). Using this model, we also found that, as suggested by a previous regional

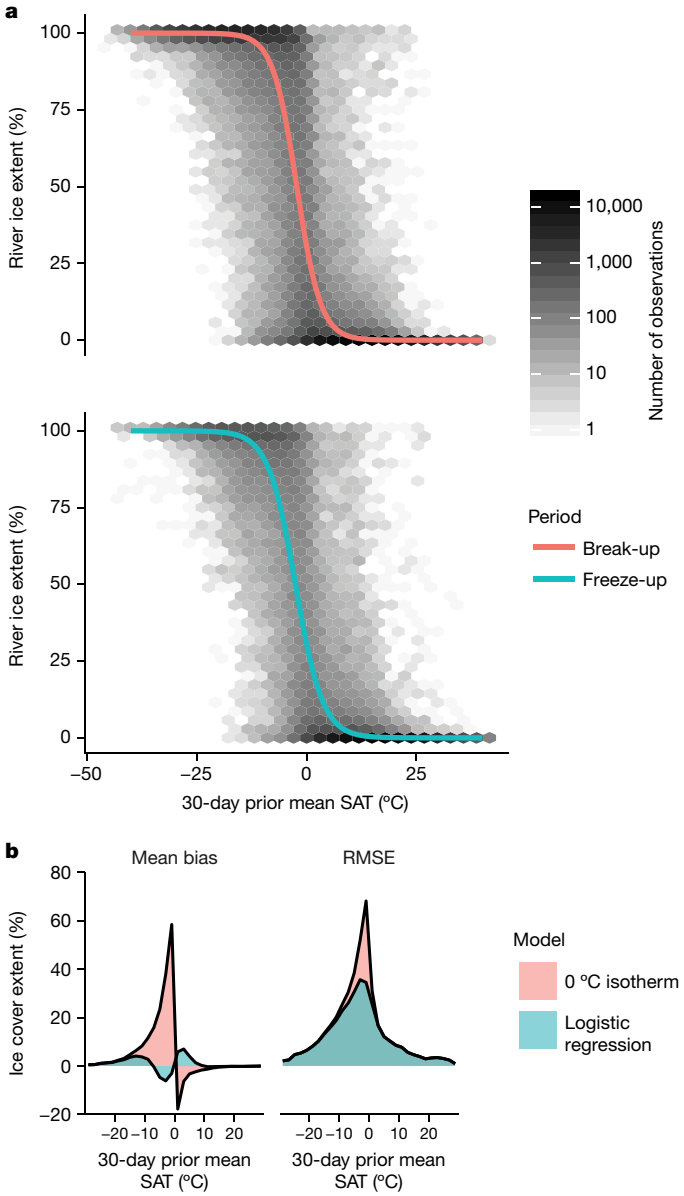

Fig. 2 | Modelling river ice extent. a, Logistic regression model (lines) constructed from the relationship between river ice extent and 30-day prior mean SAT, with the period encompassing break-up (August–January) and freeze-up (February–July) treated separately. **b**, Comparison of river ice models by mean bias and RMSE.

correlation analysis[29], SAT is a stronger control during break-up than during freeze-up.

Applying this river ice model to future SAT data for the end of the century (2080–2100) from the CESM climate model (under RCP 8.5)[30], we found that, compared with a 2009–2029 reference period (chosen to centre around the present year), monthly declines in global river ice extent ranged from 9 to 66% (0.4–9.3 percentage points) (Fig. 3 shows the changes for the Northern Hemisphere). We found a similar pattern for RCP 4.5, with a smaller magnitude of change (globally 0.2–3.2 percentage points, corresponding to a 4–35% decline, Extended Data Figs. 3, 4).

We divided the global landmass into zones defined by ice duration: ice-free (duration < 5 days), intermittent (5 days ≤ duration < 15 days), 0.5–3 months, 3–6 months and >6 months (Fig. 4a). We found substantial areal decline for regions with ice duration of >6 months and a general shift of zones with shorter ice duration to higher latitudes. Across

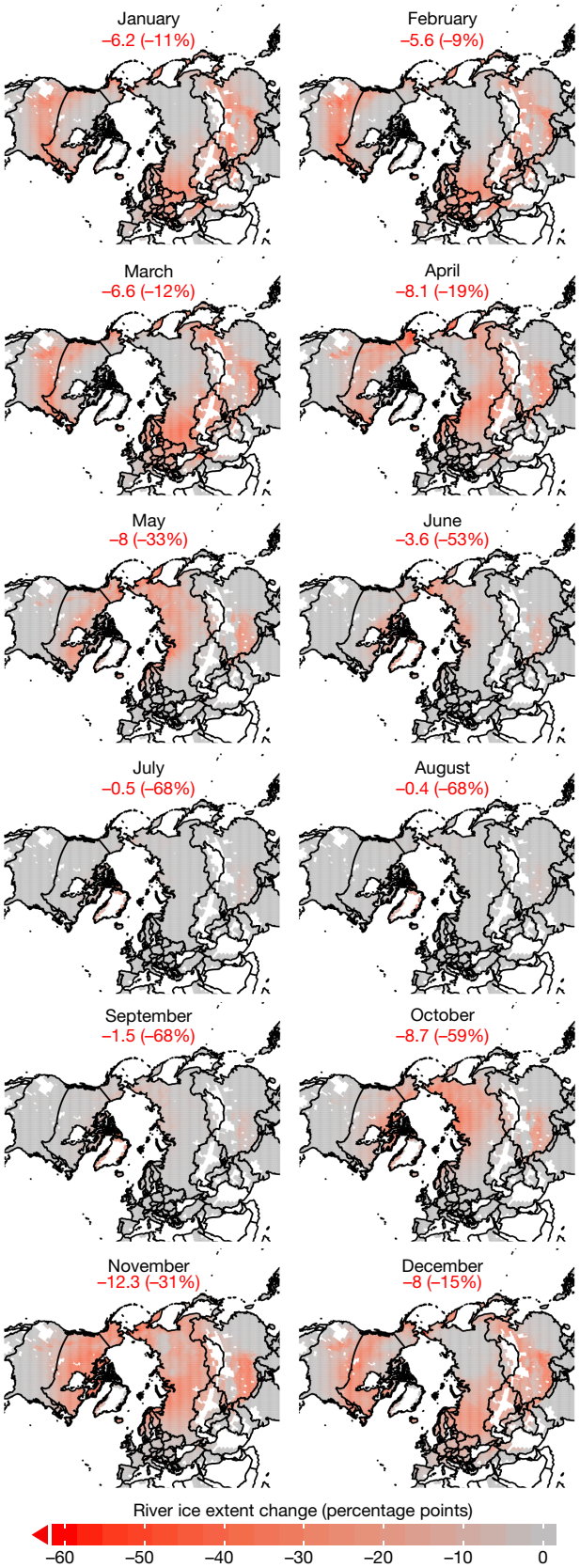

Fig. 3 | Modelled average monthly river ice difference between 2009–2029 and 2080–2100 using CESM SAT output (RCP 8.5). The percentage point change over Northern Hemisphere is shown in red, with the corresponding percentage change in parentheses. White land areas denote a lack of Landsat-observable rivers.

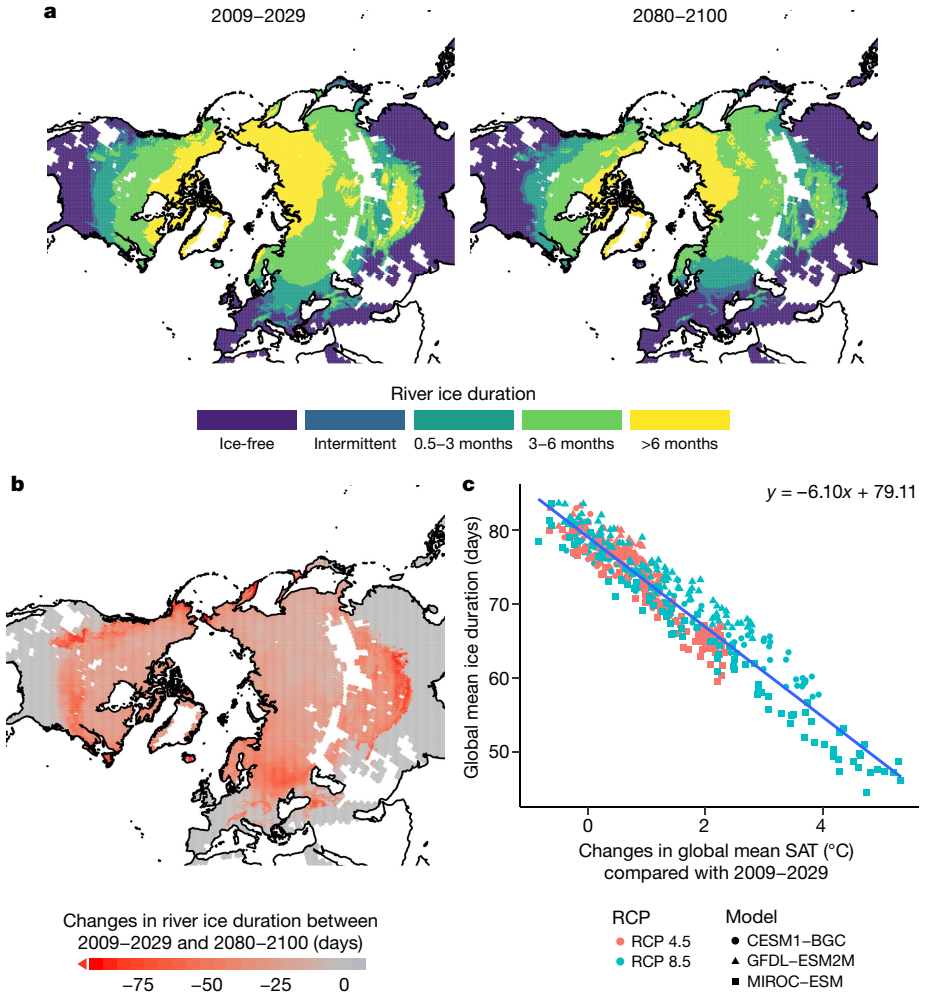

Fig. 4 | Future changes in river ice duration. a, Modelled northward shifts of ice duration zones between 2009–2029 and 2080–2100 using CESM SAT output (RCP 8.5) (see Extended Data Fig. 5 for an estimation for RCP 4.5 and for the Southern Hemisphere). White land areas denote a lack of Landsat-observable rivers. **b**, Map of changes in river ice duration between 2009–2029 and 2080–2100. **c**, The relationship between global mean river ice duration and the changes in global mean SAT.

the studied rivers, between 2009–2029 and 2080–2100, we estimated an average rate of decline in river ice duration of 23.5 days per century globally under RCP 8.5, with ice duration declining most severely in the Rocky Mountains, the northeastern United States, eastern Europe and the Tibetan Plateau (Fig. 4b). As expected, the decline in river ice duration under RCP 4.5 is less severe—the average decline in duration globally is 10.3 days per century, a rate slightly greater than that estimated for the twentieth-century Northern Hemisphere[10] (see Extended Data Fig. 5). Application of the river ice model to SAT from two other model simulations from the Coupled Model Intercomparison Project Phase 5 (CMIP5) shows a similar magnitude of change (see Methods). We also estimated the sensitivity of global river ice change to the increase in global mean SAT and found that for each 1 °C increase in global mean SAT, mean ice duration is projected to decrease by 6.10 ± 0.08 days (Fig. 4c), and the percentage of rivers affected by ice is projected to decrease by 1.48 ± 0.03 percentage points (Extended Data Fig. 6).

There are three primary implications of this study. First, our results reveal that more than half of Earth's rivers are covered by ice during the winter months, signifying a wider influence of river ice than previous estimates. As river ice is thought to impede the emission of greenhouse gases normally released by rivers[5], this upward revision implies a stronger seasonal signature in greenhouse gas emissions from the global river network. Second, projected future declines in river ice extent will transform the functions of Earth's ice-affected rivers. For example, shortening ice durations will force the transition from land-based winter transportation to waterways in the high latitudes, where a recent study suggests a 14% reduction in the land area accessible by winter roads by mid-century[6]. The loss of river ice will also substantially alter ways of living for residents of ice-affected regions in terms of the cultural ecosystem services that ice provides[8]. Finally, our results demonstrate that, globally, the mean duration and maximum extent of river ice vary approximately linearly with mean SAT for the studied range of warming. Knowing these linear rates of change enables us to quickly and accurately estimate the changes in river ice extent and duration caused by future climate change, allowing more accurate propagation of its influence on the socio-economic, hydrologic, biogeochemical and ecological processes of the global river system.

Online content

Any methods, additional references, Nature Research reporting summaries, source data, extended data, supplementary information, acknowledgements, peer review information; details of author contributions and competing interests; and statements of data and code availability are available at https://doi.org/10.1038/s41586-019-1848-1.

1. Beltaos, S. & Prowse, T. River-ice hydrology in a shrinking cryosphere. *Hydrol. Process.* **23**, 122–144 (2009).

2. Kämäri, M. et al. River ice cover influence on sediment transportation at present and under projected hydroclimatic conditions. *Hydrol. Process.* **29**, 4738–4755 (2015).
3. Prowse, T. D. River-ice ecology. I: hydrologic, geomorphic, and water-quality aspects. *J. Cold Reg. Eng.* **15**, 1–16 (2001).
4. Prowse, T. D. River-ice ecology. II: biological aspects. *J. Cold Reg. Eng.* **15**, 17–33 (2001).
5. Raymond, P. A. et al. Global carbon dioxide emissions from inland waters. *Nature* **503**, 355–359 (2013); erratum **507**, 387 (2014).
6. Stephenson, S. R., Smith, L. C. & Agnew, J. A. Divergent long-term trajectories of human access to the Arctic. *Nat. Clim. Change* **1**, 156–160 (2011).
7. Rokaya, P., Budhathoki, S. & Lindenschmidt, K.-E. Trends in the timing and magnitude of ice-jam floods in Canada. *Sci. Rep.* **8**, 5834 (2018).
8. Knoll, L. B. et al. Consequences of lake and river ice loss on cultural ecosystem services. *Limnol. Oceanogr. Lett.* **4**, 119–131 (2019).
9. Prowse, T. et al. Past and future changes in Arctic lake and river ice. *Ambio* **40**, 53–62 (2011).
10. Magnuson, J. J. et al. Historical trends in lake and river ice cover in the Northern Hemisphere. *Science* **289**, 1743–1746 (2000).
11. Prowse, T., Shrestha, R., Bonsal, B. & Dibike, Y. Changing spring air-temperature gradients along large northern rivers: implications for severity of river-ice floods. *Geophys. Res. Lett.* **37**, L19706 (2010).
12. Bennett, K. E. & Prowse, T. D. Northern Hemisphere geography of ice-covered rivers. *Hydrol. Process.* **24**, 235–240 (2010).
13. Brooks, R. N., Prowse, T. D. & O'Connell, I. J. Quantifying Northern Hemisphere freshwater ice. *Geophys. Res. Lett.* **40**, 1128–1131 (2013).
14. Brown, D. R. N. et al. Changing river ice seasonality and impacts on interior Alaskan communities. *Weather Clim. Soc.* **10**, 625–640 (2018).
15. Park, H. et al. Quantification of warming climate-induced changes in terrestrial Arctic river ice thickness and phenology. *J. Clim.* **29**, 1733–1754 (2016).
16. Ionita, M., Badaluta, C.-A., Scholz, P. & Chelcea, S. Vanishing river ice cover in the lower part of the Danube basin—signs of a changing climate. *Sci. Rep.* **8**, 7948 (2018).
17. Smith, L. C. Trends in Russian Arctic river-ice formation and breakup, 1917 to 1994. *Phys. Geogr.* **21**, 46–56 (2000).
18. Cooley, S. W. & Pavelsky, T. M. Spatial and temporal patterns in Arctic river ice breakup revealed by automated ice detection from MODIS imagery. *Remote Sens. Environ.* **175**, 310–322 (2016).
19. Pavelsky, T. M. & Smith, L. C. Spatial and temporal patterns in Arctic river ice breakup observed with MODIS and AVHRR time series. *Remote Sens. Environ.* **93**, 328–338 (2004).
20. Prowse, T., Bonsal, B. R., Duguay, C. R. & Lacroix, M. P. River-ice break-up/freeze-up: a review of climatic drivers, historical trends and future predictions. *Ann. Glaciol.* **46**, 443–451 (2007).
21. Collins, M. et al. in *Climate Change 2013: The Physical Science Basis* (eds Stocker, T. F. et al.) 1029–1136 (Cambridge Univ. Press, 2013).
22. Allen, G. H. & Pavelsky, T. M. Global extent of rivers and streams. *Science* **361**, 585–588 (2018).
23. Pekel, J.-F., Cottam, A., Gorelick, N. & Belward, A. S. High-resolution mapping of global surface water and its long-term changes. *Nature* **540**, 418–422 (2016).
24. Yamazaki, D. et al. MERIT Hydro: a high-resolution global hydrography map based on latest topography datasets. *Wat. Resour. Res.* **55**, 5053–5073 (2019).
25. Gorelick, N. et al. Google Earth Engine: planetary-scale geospatial analysis for everyone. *Remote Sens. Environ.* **202**, 18–27 (2017).
26. Zhu, Z. & Woodcock, C. E. Object-based cloud and cloud shadow detection in Landsat imagery. *Remote Sens. Environ.* **118**, 83–94 (2012).
27. Hall, D. K., Riggs, G. A. & Barton, J. S. *Algorithm Theoretical Basis Document (ATBD) for the MODIS Snow and Sea Ice-Mapping Algorithms* (NASA, 2001); https://eospso.gsfc.nasa.gov/sites/default/files/atbd/atbd_mod10.pdf
28. Copernicus Climate Change Service (C3S) *ERA5: Fifth Generation of ECMWF Atmospheric Reanalyses of the Global Climate* (C3S Climate Data Store, 2017); https://cds.climate.copernicus.eu/cdsapp#!/home
29. Lacroix, M. P., Prowse, T. D., Bonsal, B. R., Duguay, C. R. & Menard, P. River ice trends in Canada. In *13th Workshop on Ice Covered Rivers* 41–55 (Committee on River Ice Processes and the Environment, 2005).
30. Thrasher, B., Maurer, E. P., McKellar, C. & Duffy, P. B. Technical note: bias correcting climate model simulated daily temperature extremes with quantile mapping. *Hydrol. Earth Syst. Sci.* **16**, 3309–3314 (2012).

Methods

Data

Multiple datasets have been used in this study, each of which is described in detail below:

1. Global River Widths from Landsat (GRWL)[22]
2. JRC surface water occurrence[23]
3. Quality band Fmask[26] classifications of the Landsat collection 1 tier 1 images
4. ECMWF ERA5[28] surface temperature
5. NEX-GDDP climate projection SAT data[30]

GRWL[22], or Global River Widths from Landsat, is a global river database that contains 58 million river centreline locations and widths. We used the GRWL Vector Product V01.01 (dataset link: https://zenodo.org/record/1297434#.W8JkshNKh24). Specifically, we used the following properties:

- Geometry (location): expressed as point geometry with latitude and longitude in EPSG:4326 projection.
- width_m: used to identify rivers with a width of more than 90 m.
- lake_flag: indicate whether or not a centreline belongs to a river or a lake or reservoir.
- nchannel: number of channels. GRWL tends to trace the overall river centre in multichannel or braided rivers, which sometimes overlaps with islands. We only used single channel rivers (by setting nchannel = 1) in our study to avoid extracting ice status over the non-water areas.

Global surface water occurrence map[23] contains a raster map at 30 m spatial resolution with pixel values ranging from 0 to 100, indicating the percentage of times when water was detected at its location in the Landsat record. The map layer was constructed by classifying water and non-water for each of the global monthly mosaic images from Landsat 5, 7 and 8 between March 1984 and October 2015 (inclusive).

Fmask[26] is a classification algorithm designed for Landsat images to classify each pixel into five different categories (clear, water, snow/ice, cloud, cloud shadow). It is competent at classifying cloud and cloud shadow, and its classification results have been incorporated into the quality band for all Landsat collection 1 tier 1 images.

ERA5[28] is a reanalysis product that incorporates historical records of land surface and atmospheric variables into the latest modelling framework to produce a global, gridded dataset at 31 km spatial resolution. So far, ERA5 is available from 1979 at hourly or monthly temporal steps. We accessed the dataset from the European Centre for Medium-Range Weather Forecasts (ECMWF) website. We first downloaded the hourly global SAT variable (t2m) from 1 March 1984 to 31 December 2018 at a 6 h intervals (0:00, 6:00, 12:00, 18:00). We then calculated the daily mean SAT by averaging these four hourly values. Finally, we calculated the time series of mean 30-day prior temperature and spatially joined it to each of the Landsat-derived river ice observations.

NEX-GDDP, or the NASA Earth Exchange Global Daily Downscaled Climate Projections[30], is spatially downscaled to 0.25° × 0.25° from a collection of lower-resolution climate projection results developed under the CMIP5 framework. The entire collection contains model output from 21 climate models, each with RCP 4.5 and RCP 8.5 for daily minimum SAT, maximum SAT and precipitation. We calculated the daily mean SAT separately for both RCPs by taking the mean of the minimum and maximum SAT for three models—CESM1-BGC, GFDL-ESM2M and MIROC-ESM. We then calculated the daily 30-day prior mean SAT, which was then used to predict future river ice extent.

Calculating the historical river ice cover dataset

Processing GRWL for river ice cover calculation. GRWL contains approximately 58 million river centreline points globally, each including a width value. In multichannel or braided rivers, GRWL computes an effective centreline, the total flow width, and the number of channels at each centreline point. As these effective centrelines do not necessarily trace the actual river channels, we only used single channel GRWL centreline points (nchannels = 1, around 80% of rivers are single channel). Moreover, lakes and reservoirs are part of many river networks in GRWL, and the centrelines over these features are flagged. We only used non-lake centerline points in GRWL to limit the calculation of ice conditions to rivers, as ice dynamics may be different over lakes and reservoirs. Finally, while GRWL represents our latest knowledge of global river location and width, it is a static dataset, making it suboptimal for capturing ice condition on rivers over the 34 year period, during which varying degrees of morphological changes could occur. To alleviate this problem, we used only GRWL centreline points where surface water occurrence based on a previous study[23] is 90% or above, ensuring that the detected ice conditions for these points were from water surfaces. After all three filters are applied, our final river ice cover dataset used approximately 7.5 million GRWL centreline points, constituting around 271,599 km of river length. This subset of GRWL largely corresponds to Strahler–Horton stream orders greater than 3.

Constructing the global river ice cover dataset. The acquisition of the Landsat Fmask classification (cloud, cloud shadow and snow/ice) was conducted on the Google Earth Engine platform[25] for all single-channel GRWL river centreline points with water occurrence ≥90%. Specifically, we extracted the total number of centreline pixels, as well as the number of pixels covered by snow/ice, cloud and cloud shadow, for all images from Landsat TM, ETM+ and OLI sensors, ranging from March 1984 to December 2018. Then the per-image river ice fraction ($P_{\text{river\_ice}}$) and cloud fraction ($P_{\text{cloud/shadow}}$) were calculated using the following formula:

$$P_{\text{river\_ice}} = N_{\text{snow/ice}}/(N_{\text{total}} - N_{\text{cloud}} - N_{\text{shadow}})$$

$$P_{\text{cloud/shadow}} = (N_{\text{cloud}} + N_{\text{shadow}})/N_{\text{total}}$$

where N_{total}, N_{cloud}, N_{shadow} and $N_{\text{snow/ice}}$ denote the number of the total, cloud, cloud shadow and snow or ice pixels from a particular image. In total, we processed 841,365 Landsat images, covering 1984–2018. Calculating the per-image ice extent directly on Google Earth Engine greatly reduces the size of the dataset at no observable cost in terms of the details of the river ice extent required for this study.

Cleaning the river ice dataset. We systematically excluded some river ice data before calculating and modelling historical changes. To increase the stability of the river ice fraction calculation, we excluded river ice data from images for which: (1) $P_{\text{cloud/shadow}}$ is greater than 25%; (2) $N_{\text{total}} \leq 333$ (around 10 km length of river); and (3) the percentage of river pixels affected by topographic shadow exceeds 5%. This filtering reduces the data volume from 841,365 to 407,880 images.

Calculating global historical monthly mean river ice extent. We estimated global monthly mean river ice extent through two levels of spatial aggregation. For each month, we first calculated mean river ice extent for each WRS-2 tile (WRS, Worldwide Reference System) using all available Landsat-derived river ice extent observations across 34 years. Then we estimated the mean global river ice extent by calculating the weighted mean of the tile-level data. We estimated the weight for this aggregation by multiplying the length of studied rivers in the tile by the extent of overlap between the current tile and its neighbouring tiles. Specifically, we estimated the percentage of studied rivers for each WRS-2 tile using the total number of river centreline points intersecting the corresponding tile; we then estimated the degree of tile overlap (denoted by r) by calculating the proportion of non-overlapping area out of the total tile area.

$$r = (A_{\text{t}} - A_{\text{i}})/A_{\text{t}}$$

where A_{t} is the area of WRS-2 tile and A_{i} is the area of the intersection between two tiles.

The monthly weighted mean river ice extent is shown in the bar chart accompanying Fig. 1a. For each month, we also estimated the percentage of studied rivers actually captured by our satellite records. To estimate this monthly spatial coverage for each month, we divided the area of the union of all observed WRS-2 tiles for that month—representing the length of rivers observed—by the area of the union of all of the WRS-2 tiles intersecting our studied rivers. This coverage percentage was reported in the bar chart in Fig. 1a. Note that it is necessary to calculate the union of the tiles before the total covered area as there is overlap between neighbouring tiles.

Calculating historical changes in river ice extent

We assessed historical changes in river ice extent by calculating the difference in mean monthly river ice cover between two decades: March 1984–March 1994 and December 2008–December 2018—the starting and ending months were chosen to maximize the gap between the two decades. To compensate for the scarcity of Landsat records from the earlier decade and from high-latitude regions, the historical analysis—both the monthly statistics and the aggregated global map—was carried out by aggregating river ice data from the WRS-2 tile (roughly 1° × 1° at the Equator) to a 5° × 5° tile.

Calculating the global map of historical changes in river ice. To produce the map of the change in historical river ice extent for each month (Fig. 1b), we calculated the difference in mean river ice extent for each 5° × 5° tile. For each month, we kept only the tiles that contained at least five river ice observations for each of the two decades under comparison. The global map was then calculated by averaging all available monthly difference values for each tile. Monthly maps of the decadal difference in river ice extent can be found in Extended Data Fig. 2, which shows the temporal pattern of the change and the spatial coverage of the river ice record.

Calculating global historical changes in monthly mean river ice extent. To estimate the global monthly difference in river ice extent for each month, we calculated the difference in mean river ice extent for 5° × 5° tiles with at least five river ice observations for each decade. The monthly difference was then calculated by averaging the mean difference value from all available tiles, whereas the value of the observed percentage of rivers was estimated by taking the ratio between the total area of the available 5° × 5° tiles and the total area of all of the global 5° × 5° tiles that intersecting studied rivers. These statistics are shown in the bar chart in Fig. 1b.

Quantifying Landsat spatial and temporal sampling patterns. The aggregation done here to calculate historical changes in river ice could cause unintended systematic bias owing to the potential biases in the sampling time (within each month) and location (within each tile) between the two decades. We conducted the following two assessments to show that (1) both the sampling date for each month and sampling location for each 5° × 5° tile were small compared with their respective range of possible values (mean sampling time difference: −0.115 days and standard deviation: 3.4 days; mean sampling location difference: 0.012° and standard deviation: 0.41°) and (2) there was no correlation between the difference in sampling and the difference in the river ice extent, both in time and location (Pearson correlation coefficient $r_{temporal} = -0.04$ and $r_{spatial} = 0.07$). The results of these two assessments can be found in Extended Data Fig. 7.

Modelling river ice cover

Building the river ice cover model. After exploring the relationship between river ice extent and its corresponding 30-day prior mean SAT, we chose logistic regression to model their relationship. Logistic regression assumes a linear relationship between the logarithm of the odds of a phenomenon (ice) and the predictors (the 30-day prior mean SAT (SAT_{30}) and a categorical predictor we designated PERIOD), which our data follow. We used the following equations to model the river ice extent.

$$\text{odds(ice)} = N_{\text{snow/ice}}/N_{\text{water}} = P_{\text{river\_ice}}/(1 - P_{\text{river\_ice}})$$

$$\log(\text{odds(ice)}) = a\text{SAT}_{30} + b\text{SAT}_{30} \times \text{PERIOD} + c$$

The PERIOD predictor divides the data into two periods encompassing freeze-up (August–January = 0) and break-up (February–July = 1). The rationale for adding the PERIOD predictor is based on the different control strengths of temperature over ice processes between the freeze-up and breakup periods—a pattern suggested from analysis of in situ records in Canada[29].

We applied the regression model to the Landsat-derived river ice extent and ERA5-derived SAT_{30}. The parameters were estimated as $a = -0.32$, $b = -0.05$ and $c = -0.82$. Using the model, we were able to compare the strength of the control that SAT_{30} exerts on ice dynamics: we estimated that SAT_{30} control over break-up is stronger than that over freeze-up as b is negative. The entire dataset was used to assess the skill of the logistic model and the 0-°C-isotherm model (see Fig. 2b).

Projecting river ice cover at the end of the century. We projected future river ice extent by applying the river ice model to the future SAT data produced by CMIP5 climate projections. We used SAT_{30} outputs from CESM1-BGC, GFDL-ESM2M and MIROC-ESM climate simulations under both RCP 4.5 and RCP 8.5 to estimate future river ice extent and duration up to the end of the century. These models were chosen to account for potential trend biases in predicted temperature. In a similar way to evaluating the sensitivity of a model, which is common in the climate modelling community[31], we calculated the mean global SAT difference between the periods 2006–2036 and 2069–2099 for 21 models included in the CMIP5 ensemble and selected three models to represent the variabilities in relative temperature change (see Extended Data Fig. 8a). Projected future declines in river ice extent and duration are summarized in Extended Data Fig. 8b. To project future ice conditions, we calculated daily river ice extent throughout the periods 2009–2029 and 2080–2100, from which we then calculated, (1) monthly mean river ice extent and the difference between the two periods (Fig. 3, Extended Data Figs. 3, 4); (2) mean river ice duration (Fig. 4, Extended Data Fig. 5). The summary future changes in river ice extent and duration reported here were calculated by aggregating the values from the corresponding map of change at the locations of studied rivers.

Estimating the relationship between river ice condition and global mean surface temperature. For each year between 2009 and 2099, we estimated percentage of ice-affected rivers and the mean ice duration across the globe. The annual percentage of ice-affected rivers was derived by calculating the annual mean river ice extent for each studied river location, then flagging it as ice-affected if the mean value exceeded 0.041—15 days of effective ice cover over 365 days. The annual duration for each river location was estimated by counting the number of days when projected river ice extent exceeded 50%. The annual global mean surface temperature was then computed by averaging the daily mean SAT temperature across the year and then aggregating across the globe.

Sources of errors

Errors in a global dataset—especially one that quantifies highly dynamic Earth surface processes—are often unavoidable. Through building the historical river ice dataset, modelling the river ice processes and predicting future river ice conditions, we have identified three major sources of errors: errors from misclassifications in Fmask, errors in SAT values in the ERA5 dataset and errors in the projections of future river ice condition.

Qualitative evaluation of Fmask snow/ice classification. To qualitatively assess the accuracy of the Fmask snow/ice classification, we randomly selected—stratified sampling by temperature range and observed river ice cover—160 images for visual evaluation. We found that snow/ice classification is adversely affected in the following situations (from the most to the least frequent):

- Commission error in classifying turbid water as snow/ice—found mostly over the Yellow River in China and Amu Darya in Turkmenistan. Less frequently found over the Red River, Arkansas River and Missouri River in the United States.
- Commission error in classifying cloud as snow/ice—no strong spatial pattern found for this type of error.
- Omission error in classifying topographically shaded snow/ice as water.
- Omission error in classifying thin ice as water—this type of error is rare and mostly observed on still portions of rivers (such as reservoirs and lakes, which are not used in this analysis).

Evaluating Landsat-derived river ice extent. We use the US Geological Survey's quality band snow/ice classification to derived river ice extent. The snow/ice classification is calculated using Fmask[26]. Fmask classifies each pixel of the Landsat image into one of five classes. Although Fmask is considered the most accurate[31] cloud classification algorithm for Landsat images, its snow/ice classification has not been evaluated for accuracy. Here we used in situ reported river ice conditions to evaluate the accuracy of river ice extent calculated using Fmask.

Although direct in situ river ice records are scarce, we were able to obtain the river ice status for the state of Alaska, United States, from the archive of the National Weather Service (NWS). We also inferred river ice conditions using the backwater flag that accompanies the daily gauge flow records from Water Survey of Canada (WSC). The backwater flag was used in previous studies as strong indicator of ice conditions[32].

In the following, we first explain our approach to extracting and cleaning the in situ datasets. We then introduce our method for calculating the river ice extent from Landsat images and matching it to the in situ observations. Finally, we show the results of the evaluations.

NWS river ice observations. We obtained historical records for 485 stations in Alaska from S. Lindsey at the Alaska-Pacific River Forecast Center. We encountered two challenges in using this dataset for evaluation. First, the files we obtained, while containing ice observations and station descriptions, do not contain the geolocations of these stations. Fortunately, the station description often followed the 'river_name_at/near_location_name' naming convention (for example, 'Yukon River at Beaver'). We were able to manually identify 177 stations that have both freeze-up and break-up information for at least one water year, 115 of which we successfully georeferenced and 13 of which we eventually used for evaluation after excluding sites that either are close to a river that is too small for Landsat to observe or did not have records that temporally overlapped with the Landsat observation. Second, NWS reported multiple thresholds that indicate various ice conditions during both the freeze-up and break-up periods. However, there were varying amounts of missing data for these dates. For example, while the NWS directly reported freeze-up date, the majority of the values in this field were missing data, which rendered it of very limited value. Instead, we used the first ice date as the dates of ice onset and 'breakup' as the date of ice-off.

WSC flag. The WSC includes flags in its daily discharge data that indicate the state of flow conditions. Among these flags, the backwater flag or 'B' flag is used to indicate ice conditions[32]. In our evaluation, we followed existing practice, treating dates with B flags as dates of river ice cover.

Matching in situ ice coverage with Landsat-derived ice coverage. After merging the geolocations of the NWS stations and the WSC stations, we calculated the river ice conditions for these locations according to Fmask classifications. Specifically, for each in situ location, we calculated the Fmask-derived river ice extent for GRWL rivers (nchannel = 1; lake_flag = 0; width_mean ≥ 90 m) located within a 1,500-m radius of the gauge.

To evaluate the Landsat-derived ice coverage against the in situ records, we matched the datasets spatially (to the 1,500 m proximity of each station) and temporally (to the same day). The same-day temporal matching was straightforward for WSC records, as they reported daily ice conditions. However, as the NWS reported only dates of ice-on and ice-off, we treated dates that fell between an ice-on date and the following ice-off date as ice-covered dates, and those that fell between an ice-off and the following ice-on date as ice-free dates. In total, we matched 18,930 pairs (NWS-Alaska: 515 pairs over 13 sites; WSC: 18,415 pairs over 139 sites) of in situ and Landsat-derived river ice observation for our evaluation.

Evaluating Landsat-derived river ice coverage. When comparing the Landsat-derived river ice coverage to that reported from the field, we first converted the continuous values (0–100%) to a binary ice condition using a threshold of 50%—ice coverage ≥50% is classified as 'ice-covered' and <50% is classified as 'ice-free'. The 50% threshold was chosen as we found that that threshold choice had little impact on the final evaluation. Then we calculated the accuracy, sensitivity and specificity by constructing a confusion matrix using the in situ reported ice condition as a reference and the Landsat-derived ice state as the observation. Overall, Landsat-derived river ice coverage was highly consistent with the in situ reports (accuracy = 0.94, sensitivity = 0.91, specificity = 0.96, Extended Data Fig. 9). When the analysis was broken down into monthly evaluations, accuracy was highest during summer months (June–August: mean accuracy: 0.98) and lower during the remaining months, with no particular seasonal pattern (accuracy: 0.8–1.0 with mean accuracy 0.91, Extended Data Fig. 9b). Reduced accuracy occurred during months when river ice was present and was attributed to: (1) complicated reflectance returns due to dynamic transition between ice and water; (2) increased turbidity accompanying ice break-up; (3) the difference in scale between the Landsat-derived ice condition (averaging across a 1,500-m radius) and the in situ records (scale unknown, see examples in Extended Data Fig. 9c); and (4) errors in the in situ records. Notably, the accuracy derived from the observation-based NWS ice conditions (overall accuracy: 0.97) was generally higher than that from the WSC (overall accuracy: 0.94) (see also Extended Data Fig. 9b). The fact that the ice condition from the WSC was inferred, instead of observed, could have contributed to this discrepancy.

Comparison with in situ river ice records also showed no systematic differences among Landsat sensors. Accuracy was similar across data from Landsat 5 (TM), Landsat 7 (ETM+) and Landsat 8 (OLI) (see Extended Data Table 1). It is worth noting that Landsat 8 has an extra flag for cirrus clouds, which could potentially improve the quality of ice data by better excluding cloud-affected observations. However, we decided not to use this flag, as its inclusion could potentially cause varying data quality between sensors, which then could compromise the detection of historical river ice change.

Human influence on river ice. Human activities that affect rivers—such as river engineering and water pollution—tend to systematically and permanently alter the river morphology, as well as the thermal and physical properties of the flow. River ice regimes affected by these influences cannot be explained by the changes in SAT alone. In one previous study, human activity was found to affect the river ice regime to a much greater degree than climate variation along two highly regulated river reaches in Europe[33]. While we acknowledge the contribution of these non-climatic factors, quantification of their effects globally exceeds the scope of this study. Nonetheless, interpretation of our results in rivers/regions that are known to be heavily engineered requires extra caution.

Although direct anthropogenic influence on river ice regimes should be considered when interpreting both in situ and remotely sensed data, interpreting remotely sensed data requires extra consideration

of the sensitivity of the classification algorithms to anthropogenic influence. Otherwise, there is a risk of falsely attributing changes in river ice to changing climate. For example, for the lower Yellow River, our detection of great historical river ice decline is likely to be largely due to the combined effect of changes in water turbidity—mostly owing to recent damming upstream—and the tendency for Fmask to falsely classify turbid water as snow/ice.

Uncertainties in ERA5 SAT. Because it was released very recently, there is no spatially comprehensive evaluation of SAT in ERA5, so its overall accuracy remains unknown. However, from studies that evaluated this parameter regionally, ERA5 has outperformed other reanalysis datasets and can accurately represent the magnitude and variability of near-surface air temperature over Antarctica[34].

Spatial scale mismatch between temperature dataset and river size. When attaching the ERA5 temperature data (spatial resolution of approximately 30 km) to our river ice extent dataset and modelling river ice based on the merged dataset, as well as predicting future river ice extent with temperature data from NEX-GDDP (spatial resolution 0.25°), we implicitly assumed that temperature for a grid cell is representative of that experienced by the river in it. This assumption could result in bias when mixing temperatures from land and water pixels, especially when large topographic variability exists in the grid cell, as rivers tend to flow along topographic low areas, and elevation greatly affects temperature. The degree of this inherent systematic bias may be reduced in the future with the development of more advanced reanalysis datasets.

Data availability

The global river ice dataset can be accessed at https://doi.org/10.5281/zenodo.3372709. The in situ and Landsat-derived river ice records for evaluating ice classification can be accessed at https://doi.org/10.5281/zenodo.3372754.

Code availability

The code used to acquire, analyse and visualize the dataset can be accessed online at the project's GitHub page (https://github.com/seanyx/global-river-ice-dataset-from-Landsat). The river ice model and all figures in the paper (including the extended data figures) were made using R statistical software (http://www.R-project.org/).

31. Foga, S. et al. Cloud detection algorithm comparison and validation for operational Landsat data products. *Remote Sens. Environ.* **194**, 379–390 (2017).
32. Beaton, A., Whaley, R., Corston, K. & Kenny, F. Identifying historic river ice breakup timing using MODIS and Google Earth Engine in support of operational flood monitoring in Northern Ontario. *Remote Sens. Environ.* **224**, 352–364 (2019).
33. Takács, K., Kern, Z. & Nagy, B. Impacts of anthropogenic effects on river ice regime: examples from Eastern Central Europe. *Quat. Int.* **293**, 275–282 (2013).
34. Gossart, A. et al. An evaluation of surface climatology in state-of-the-art reanalyses over the Antarctic Ice Sheet. *J. Clim.* **32**, 6899–6915 (2019).

Acknowledgements Funding was provided to T.M.P. by a subcontract from the SWOT Project Office at the NASA/Caltech Jet Propulsion Laboratory. We thank S. Lindsey at the Alaska-Pacific River Forecast Center for providing us with the NWS Alaska river break-up and freeze-up records, and W. Dolan for help with geolocating Alaskan river ice records.

Author contributions X.Y. developed the method, performed analysis and drafted the manuscript. T.M.P. conceptualized the study, assisted with analysis and reviewed and edited the manuscript. G.H.A. provided the GRWL dataset and reviewed and edited the manuscript.

Competing interests The authors declare no competing interests.

Additional information
Correspondence and requests for materials should be addressed to X.Y.
Peer review information *Nature* thanks John Kimball, Gerhard Krinner and Homa Kheyrollah Pour for their contribution to the peer review of this work.

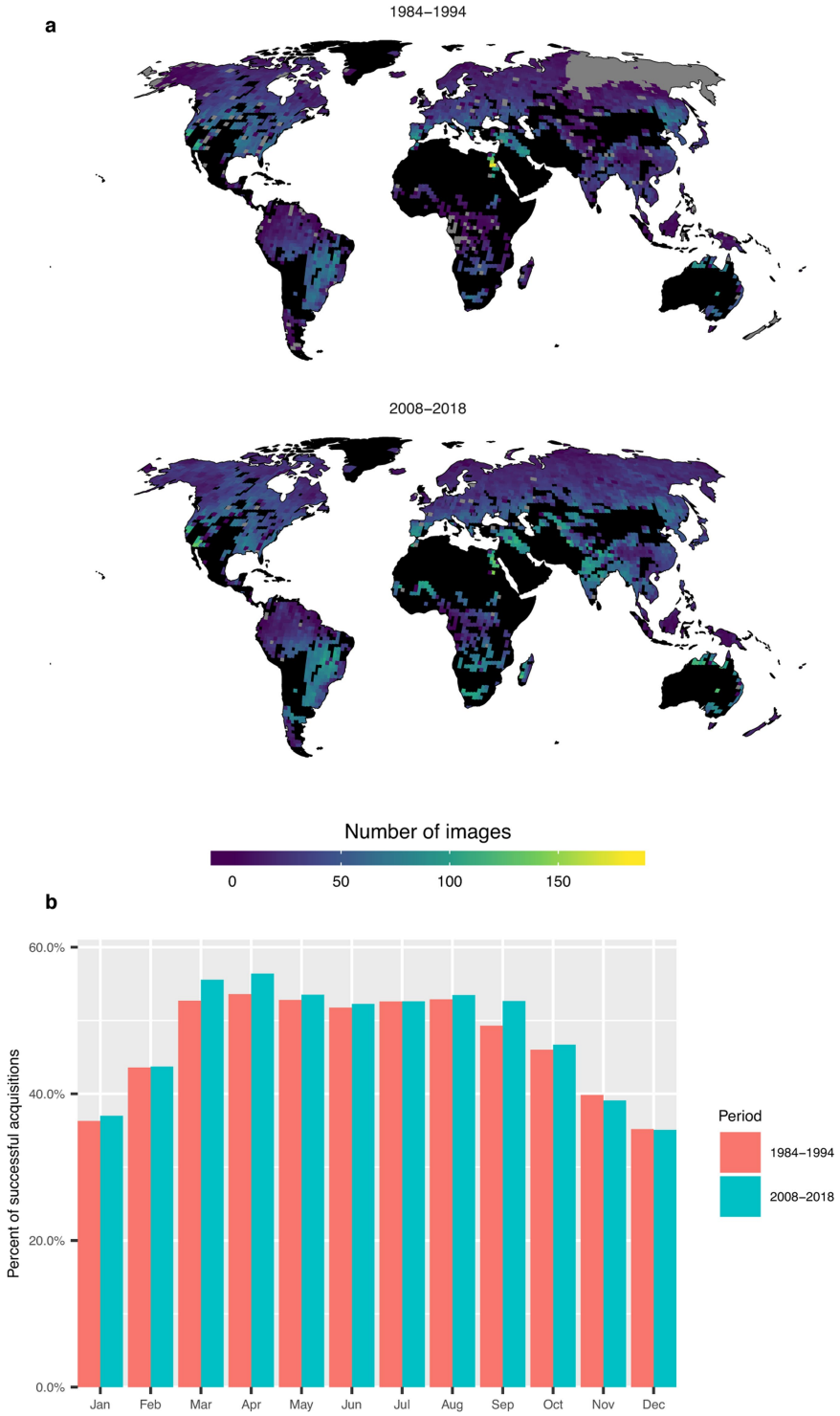

Extended Data Fig. 1 | Data availability between two historical decades. **a**, Data availability map for the decades 1984–1994 and 2008–2018 based on the river ice extent dataset. Black indicates no data or no studied river. **b**, Percentage of successful river ice observations for each month of each decade. The percentage was calculated by taking the ratio between the number of observations used in the historical analysis and the total number of Landsat river observations when no filters (cloud, topographic shadow and river length) were applied.

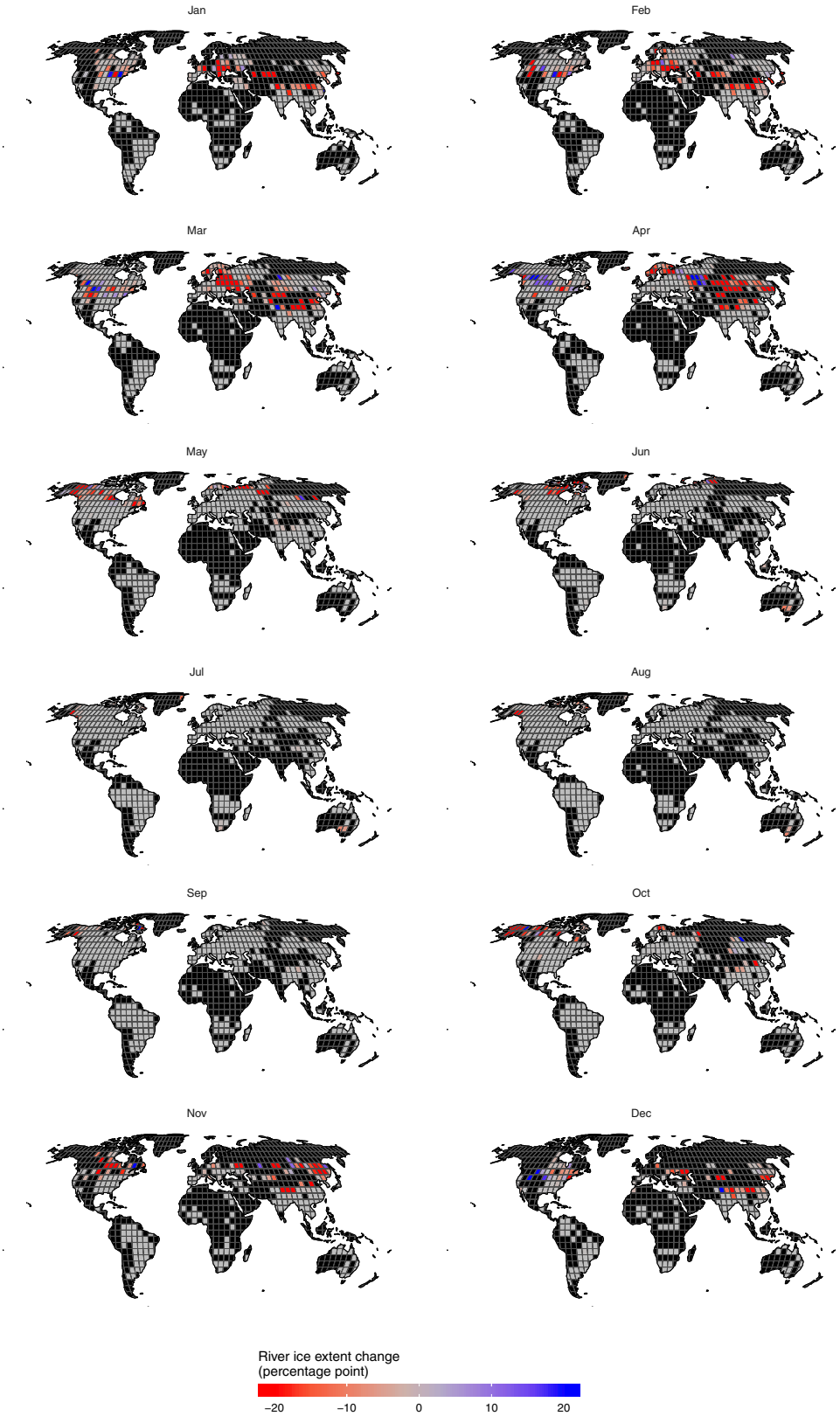

Extended Data Fig. 2 | Monthly maps of the changes in river ice extent between 1984–1994 and 2008–2018. Black indicates no data or no studied river.

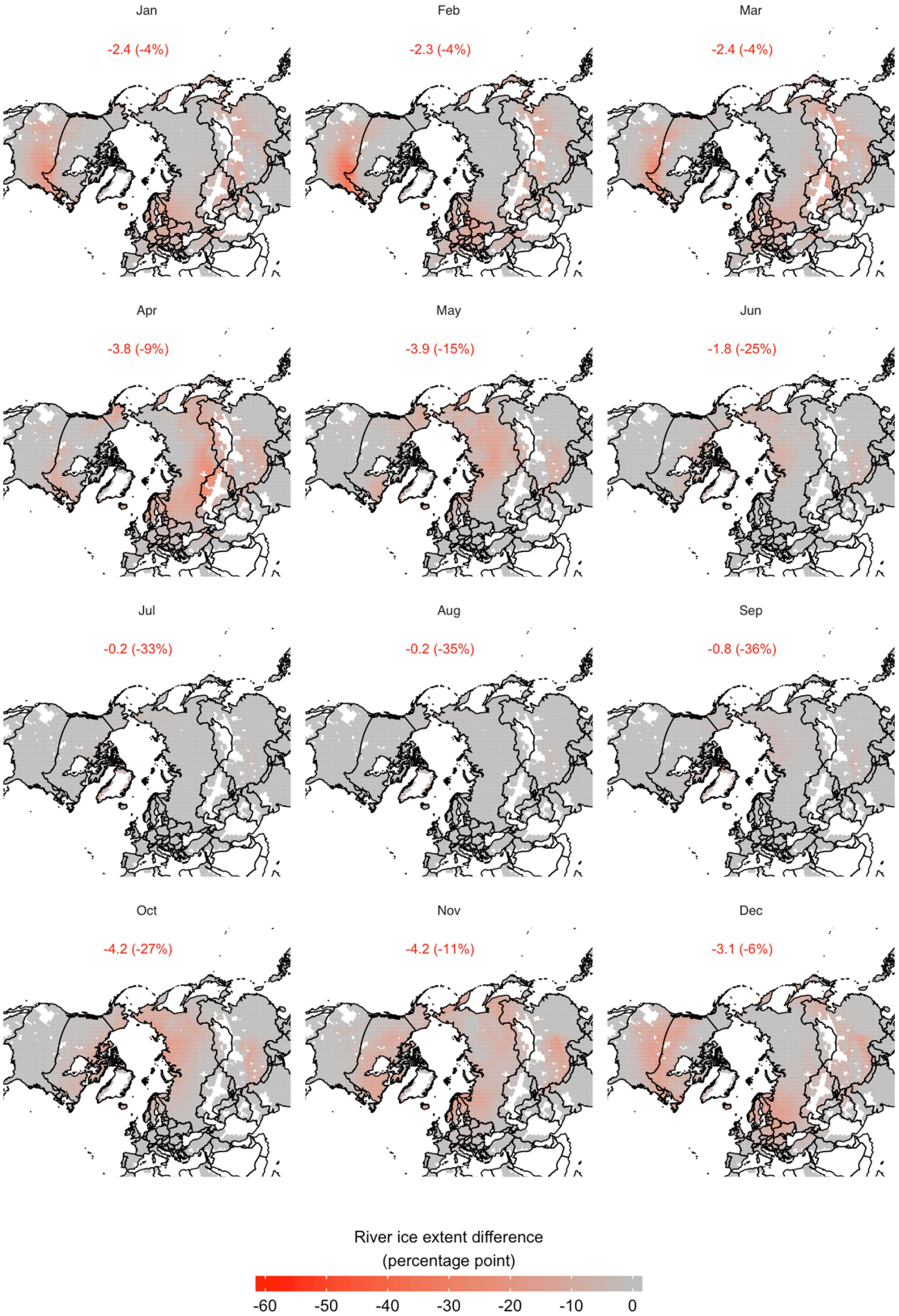

Extended Data Fig. 3 | Modelled average monthly river ice difference between 2009–2029 and 2080–2100 using CESM SAT output (RCP 4.5). The percentage point change over the Northern Hemisphere is listed under the month, with the percentage change in parentheses.

a

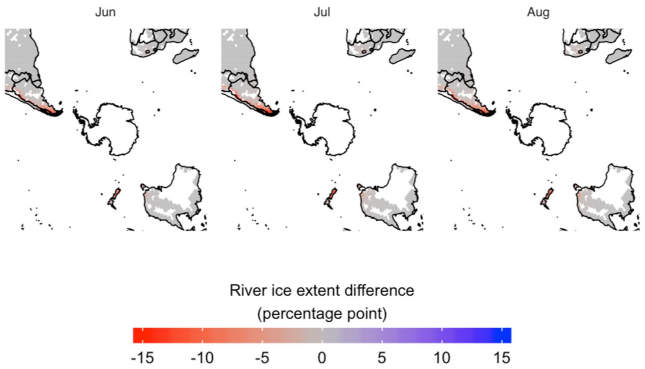

Month	Percentage point change	Percent change
Jan	-0.03	-61%
Feb	-0.02	-64%
Mar	-0.02	-65%
Apr	-0.05	-65%
May	-0.13	-61%
Jun	-0.3	-57%
Jul	-0.43	-55%
Aug	-0.39	-51%
Sep	-0.27	-50%
Oct	-0.16	-53%
Nov	-0.09	-58%
Dec	-0.05	-58%

b

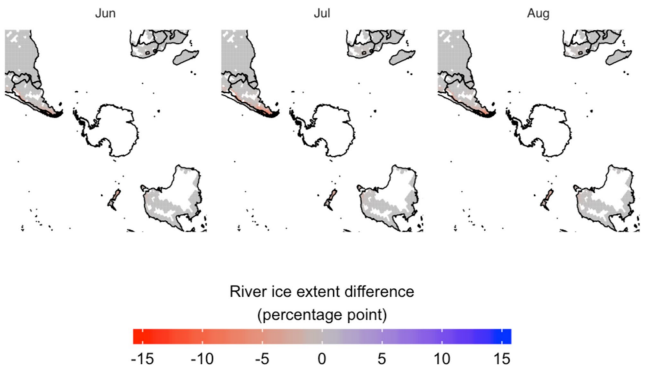

Month	Percentage point change	Percent change
Jan	-0.01	-25%
Feb	-0.01	-28%
Mar	-0.01	-31%
Apr	-0.02	-23%
May	-0.04	-22%
Jun	-0.09	-18%
Jul	-0.19	-24%
Aug	-0.15	-20%
Sep	-0.09	-17%
Oct	-0.07	-24%
Nov	-0.03	-23%
Dec	-0.02	-25%

Extended Data Fig. 4 | Modelled average monthly river ice difference between 2009–2029 and 2080–2100 using CESM SAT. a, Model output under RCP 8.5. **b**, Model output under RCP 4.5. Only the months that showed obvious changes in percentage points (June, July and and August) were mapped. The percentage point changes and percentage changes over the Southern Hemisphere are listed in the tables on the right.

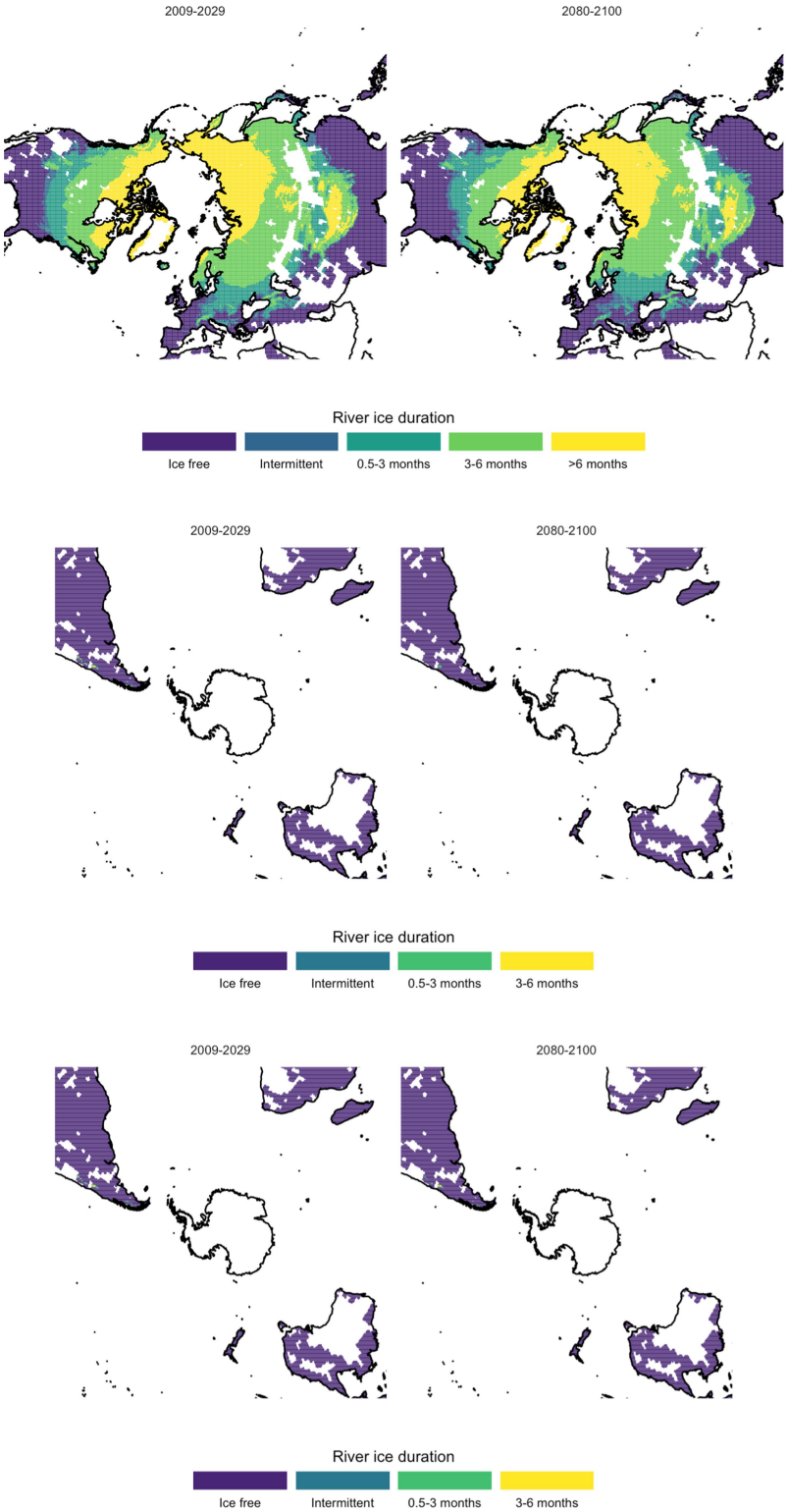

Extended Data Fig. 5 | Modelled ice duration zones between 2009–2029 and 2080–2100 using CESM modelled SAT. a, The Northern Hemisphere under RCP 4.5. **b**, **c**, The Southern Hemisphere under RCP 8.5 (**b**) and RCP 4.5 (**c**). Areas showing obvious changes are marked by red rectangles.

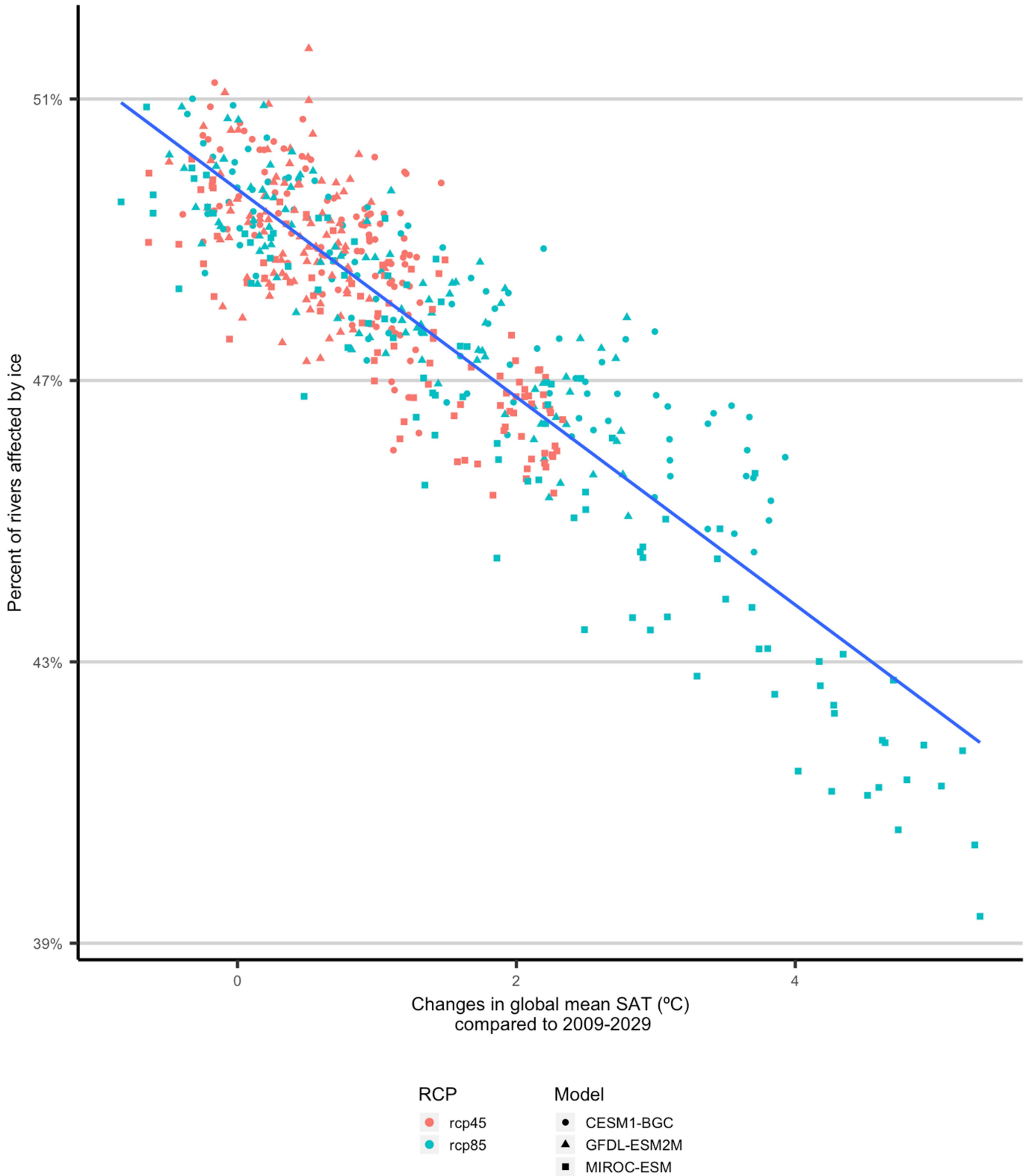

Extended Data Fig. 6 | Sensitivity of the changes in annual maximum river ice extent to the changes in global mean SAT. The sensitivity was assessed for three models (CESM1-BGC, GFDL-ESM2M and MIROC-ESM).

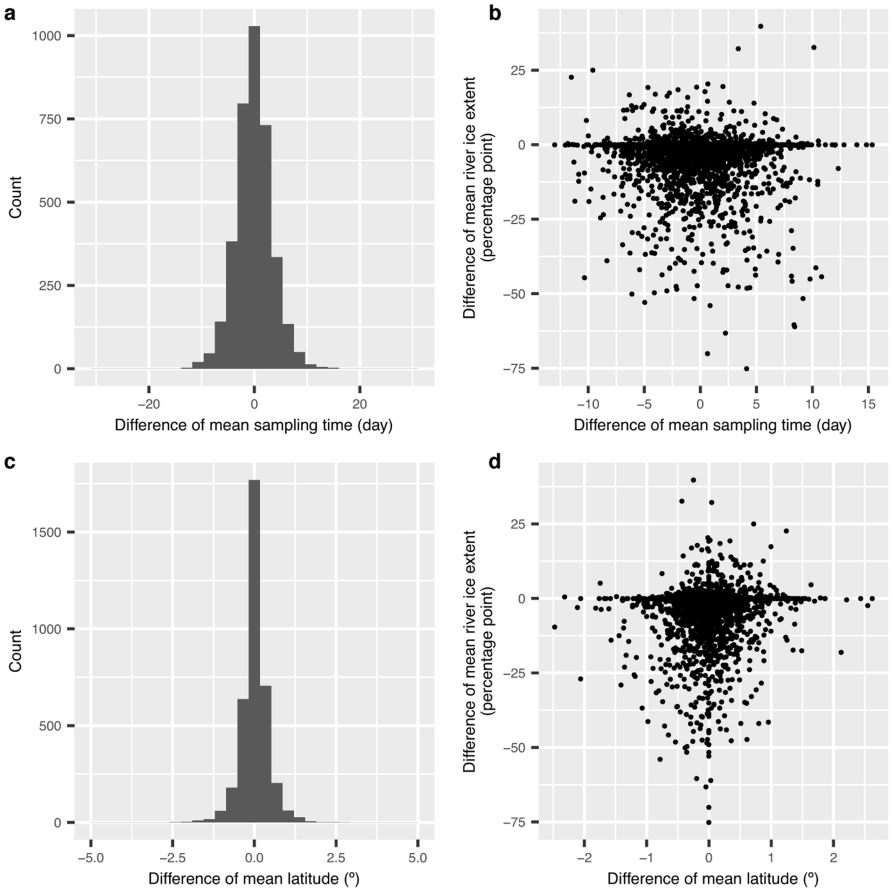

Extended Data Fig. 7 | Landsat sampling difference between the historical period 1984–1994 and 2008–2018. a, Distribution of the temporal sampling difference within each month. **b**, Temporal sampling difference and its relationship with the difference in the ice extent. **c**, Distribution of the spatial sampling difference within the 5° × 5° tiles. **d**, Spatial sampling difference and its relationship with the difference in the ice extent.

a

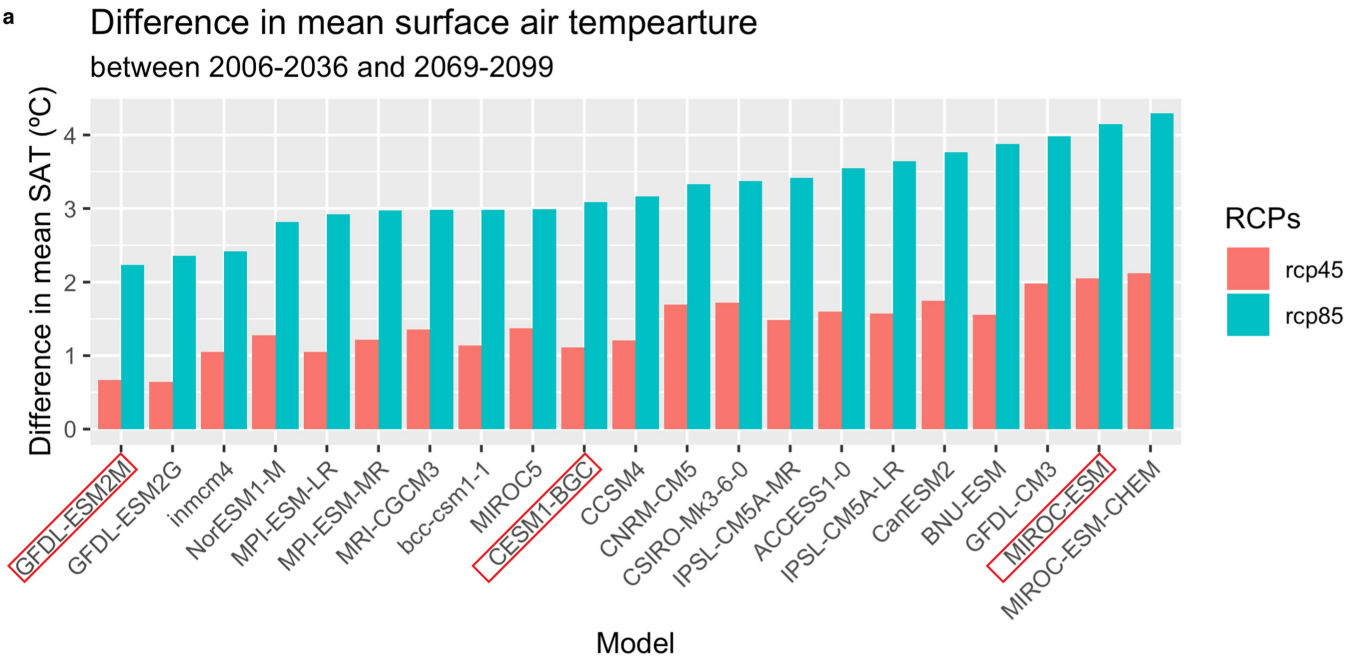

b

Model	**RCP**	**Duration Difference (days)**	**Global mean SAT difference (°C)**
CESM1-BGC	8.5	-16.7	3.43
GFDL-ESM2M	8.5	-12.5	2.45
MIROC-ESM	8.5	-28.4	4.59
CESM1-BGC	4.5	-7.3	1.19
GFDL-ESM2M	4.5	-2.7	0.66
MIROC-ESM	4.5	-12.9	2.15

Extended Data Fig. 8 | Summary of river ice duration decline based on temperature outputs from three CMIP5 models. a, Difference in the global mean SAT across 21 CMIP5 models between 2006–2036 and 2069–2099. The three models used to assess future river ice change are marked with red rectangles. **b**, Decline in global mean river ice duration between 2009–2029 and 2080–2100 for the three selected models.

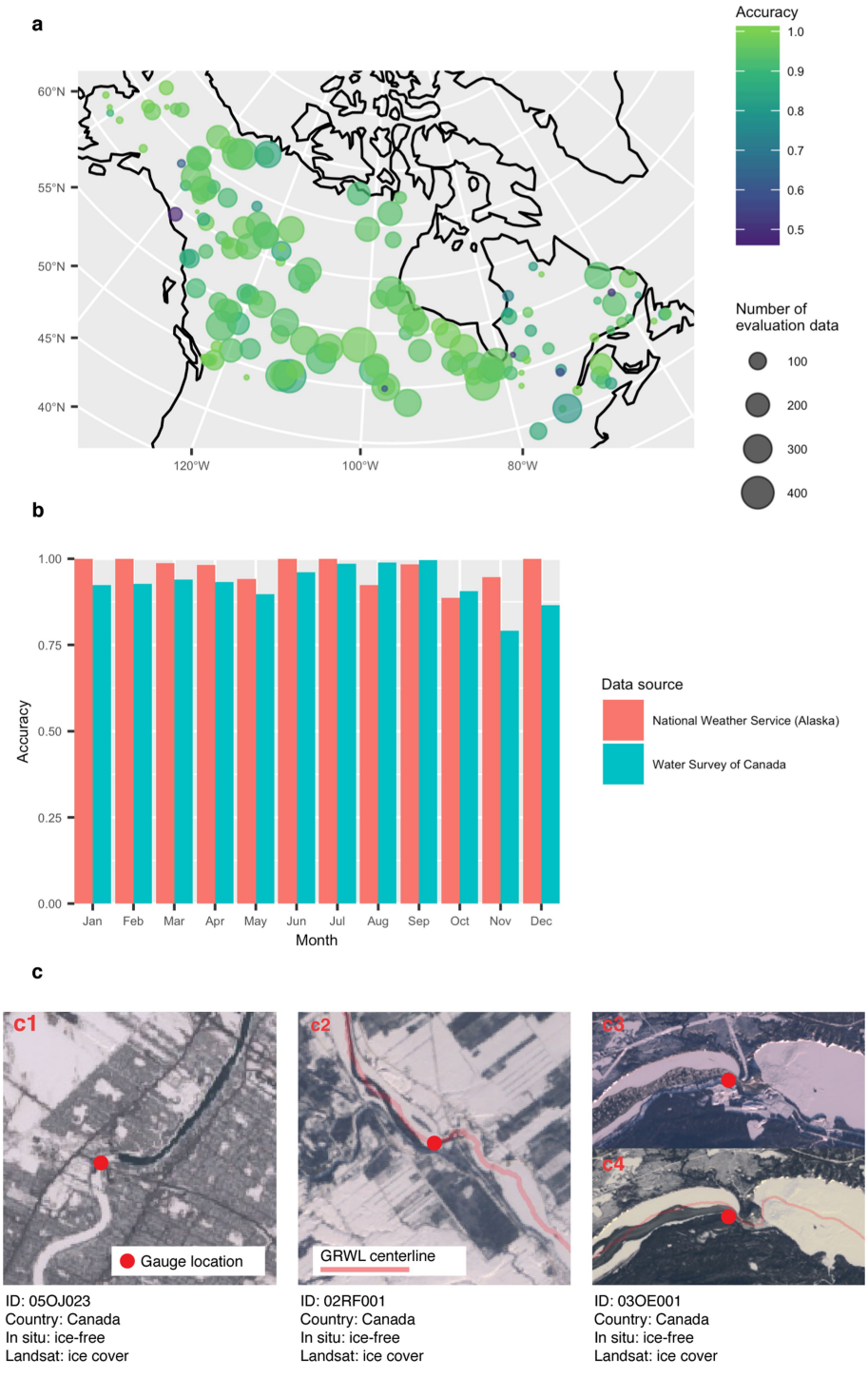

Extended Data Fig. 9 | Evaluating Landsat-derived river ice conditions against in situ river ice records. a, The accuracy of Landsat-derived river ice extents when evaluated against in situ reports of river ice condition. **b**, Monthly evaluation of Landsat-derived river ice estimates. **c**, Examples of differences in definition between remotely sensed and ground-based ice conditions. The GRWL centrelines are shown in images c2 and c4 to indicate the river. Satellite images courtesy of the US Geological Survey.

Extended Data Table 1 | Fmask-derived river ice evaluation across Landsat missions

Sensor	Accuracy	Specificity	Sensitivity	% of data
TM	0.943	0.957	0.919	72.3%
ETM+	0.933	0.943	0.922	12%
OLI	0.941	0.976	0.907	15.8%